Journal of Materials Chemistry A

Accepted Manuscript

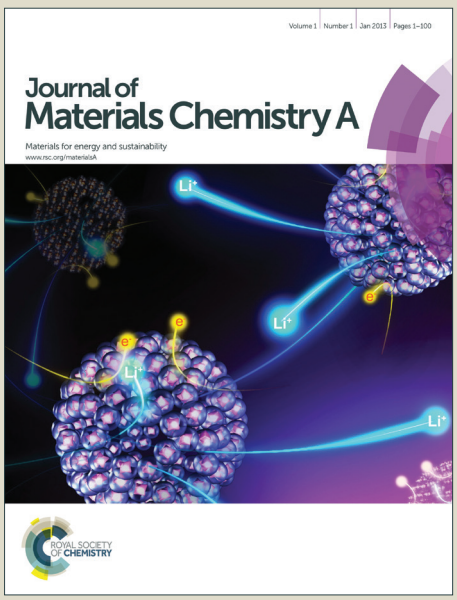

ROYAL SOCIETY OF CHEMISTRY

www.rsc.org/materialsA

Photochemical synthesis of ZnO/Ag_2O heterostructures with enhanced ultraviolet and visible photocatalytic activity

Shuaishuai Ma,‡ Jinjuan Xue, ‡ Yuming Zhou, * Zewu Zhang

School of Chemistry and Chemical Engineering, Southeast University, Nanjing 211189, P. R. China

Abstract: ZnO/Ag_2O heterostructures were successfully synthesized via a simple one-step photochemical rout. The sample was characterized by X-ray diffraction (XRD), transmission electron microscopy (TEM), and energy dispersive X-ray analysis (EDX). The photocatalytic activity toward degradation of methylene blue (MB) aqueous solution both under ultraviolet (UV) and visible-light were investigated. The results showed that the as-prepared ZnO/Ag_2O heterostructures significantly enhanced the UV and visible photocatalytic activity compared to pure ZnO and Ag_2O. In particular, the rate of degradation of the as-prepared ZnO/Ag_2O heterostructures was 27.4 and 15.6 times faster than that of using bare ZnO nanoparticles under the UV and visible light irradiation, respectively. Furthermore, the ZnO/Ag_2O heterostructures could be easily recycled in UV and visible photocatalytic activity due to the low concentration of surface defects in the as-prepared ZnO/Ag_2O heterostructures. Moreover, the ZnO/Ag_2O heterostructures could also degrade MB dye in different water sources like Changjiang river water and tap water with high efficiency as well as in deionized water and that will greatly promote their application in the area of environmental remediation.

* Corresponding author. Tel.: +86 25 52090617; fax: +86 25 52090617.
E-mail address: ymzhou@seu.edu.cn (Yuming Zhou).
‡S.S. Ma and J.J. Xue contributed equally to this work.

Introduction

In decades, environmental problems such as organic pollutants and toxic water pollutants produced by some industries have become more and more harmful to human health.[1-3] Photocatalysis is a promising technique for solving many current environmental and energy issues through its efficiency and broad applicability.[4] With the steady and fast growing field of nanoscience and nanotechnology, nanostructured semiconductor photocatalysis has attracted a great deal of attentions due to their wide application to environmental remediation, especially for organic pollutants removal.[5-8] Among the semiconductors, Zinc oxide (ZnO), owing to its low cost, ease in preparation, environmental abundance, and nontoxicity, is considered to be one of the most important semiconductors being harnessed in photoinduced applications such as photodetection and photocatalysis.[9-12] However, ZnO is a wide band gap (3.37 eV) semiconductor with inevitable shortcomings for photocatalysis-based applications. Such photocatalysts only active under UV irradiation but often with low photocatalytic efficiency and high rate of photocorrosion. Also, nanosized ZnO materials are normally unstable, easy to be agglomerated and difficult to recovery after use.[13] Thus, the solvable issue is through preparation of photocatalytic materials with the visible light absorption characteristic, doping with metallic or non-metallic elements, metal oxides, carbon materials, sensitizing by dye, and preparing composites with narrow bandgap semiconductor materials.[14-17] Among them, semiconductor-noble metal type nanoheterostructures are one of the most

promising hybrid materials to be extensively investigated due to the fact that they may enhance the photocatalysis efficiency from the dramatically reduced electron-hole recombination rate.[18] Usually, a metal and a semiconductor would form Schottky barriers at their interfaces because of their differences in work function and band alignment, leading to the obvious separation and transfer of photoexcited charges.[19] To date, researchers have found that ZnO based heterojunction, such as deposited noble metals (Ag, Au, Pt, or Pd) on the ZnO surface and semiconductor (CdS, ZnS, V_2O_5, Ag_2O) couple with ZnO, could effectively improve photocatalytic efficiency.[20-26]

Ag_2O, a brown powder possessing a simple cubic structure with a lattice parameter of 0.472 nm, has been widely used in many industrial fields, as cleaning agents, preservatives, colorants, electrode materials, and catalysts for alkane activation and olefin epoxidation.[27, 28] The band-gap energy of Ag_2O is reported to be 1.2 eV with an energy level of CB edge of + 0.2 eV (vs. SHE).[29] Also, Ag_2O is a p-type semiconductor.[30] All these properties of Ag_2O are beneficial for the formation of p-n nanoheterojunction with ZnO for superior photocatalyst. The photogenerated electrons can move to the conduction band of n-type ZnO and photogenerated holes can move to the valence band of p-type Ag_2O which promote an interfacial electron transfer process and reduce the charge recombination on the semiconductor. On the other hand, owe to its narrower band gap (1.2 eV) relative to ZnO, Ag_2O nanoparticles are able to act as efficient photosensitizers under solar light irradiation and enhance the visible photocatalytic performance of ZnO. However, to the best of our knowledge, the studies on the ZnO/Ag_2O system are extremely scanty and the synthetic approaches are complex.[26, 31]

Herein, for the first time, we applied a photochemical technique to successfully synthesize ZnO/Ag_2O heterostructures. This method is simple and cost-effective without any expensive equipment, complex process control, and stringent reaction conditions. The prepared samples were characterized by X-ray diffraction (XRD), scanning electron microscopy (SEM) couple with energy-dispersive X-ray spectroscopy (EDS), transmission electron microscopy (TEM) and high resolution transmission electron microscopy (HRTEM). Meanwhile, a possible formation mechanism of the as-prepared ZnO/Ag_2O heterostructures is proposed. The photocatalytic activity of the ZnO/Ag_2O heterostructures was carefully investigated by degradation of methylene blue (MB) dye under UV and visible irradiation. The results indicated that the as-preparaed ZnO/Ag_2O heterostructures exhibit much higher UV and visible photocatalytic activity than that of bare ZnO and Ag_2O nanoparticles. Furthermore, the two different photocatalytic mechanisms of ZnO/Ag_2O heterostructures under UV and visible-light irradiation were illustrated and discussed.

Experimental section

Preparation of ZnO/Ag_2O heterostructures

Silver nitrate ($AgNO_3$), ethanol (EtOH) and methylene blue (MB, $C_{16}H_{18}ClN_3S$) were purchased from Aladdin Chemical Regent Co., Ltd. (Shanghai, China), and commercial Zinc oxide (ZnO) was purchased from Maoye Chemical Regent Co., Ltd. (Chongqing, China). All the reagents in this experiment are analytically pure and used without further purification. In a typical procedure, 2.4 mmol $AgNO_3$ was added into 100

ml deionized water to form aqueous solution, then 3 mmol commercial ZnO was dispersed in the $AgNO_3$ solution. The suspention was stirred for 1 h in the absence of light to reach complete adsorption for Ag^+ ions on the surface of ZnO nanoparticles, then irradiated with a 250W high-pressure mercury lamp (λ = 365 nm) for 15 min with stirring. The resulting product was obtained by centrifugation, then washed with deionized water for several times and finally dried under vacuum.

Sample characterizations

The morphology of the sample was examined with scanning electron microscope (SEM, JEOL JSM-6510LV) coupled with an energy-dispersive X-ray spectroscopy (EDS, Oxford instruments X-Max), transmission electron microscope (TEM, FEI Tecnai F20), and high resolution TEM (HRTEM). The crystallinity and phase of the products were determined by X-ray diffraction (XRD, Rigaku Ultima Ⅳ, Cu Kα radiation). The nitrogen adsorption and desorption isotherms were measured at 77 K on an ASAP 2020 (Micromertics USA). PL spectra were measured using room temperature photoluminescence with a 325 nm He–Cd laser excitation wavelength (Shimadzu RF-5301). UV-vis diffuse reflectance spectra (DRS) of the samples were recorded on a UV-vis spectrophotometer (UV-3600, Shimadzu) with an integrating sphere attachment.

Evaluation of Photocatalytic Performance

20 mg ZnO/Ag_2O heterostructures were added into 100 mL of 3.12×10^{-5} mol/L MB solution. A 250 W UV lamp with maximum emission at 365 nm was used as UV light source and a 500 W xenon lamp of which main wavelength lies in 365-720 nm was used as

the visible light source. Before irradiation, the solution was stirred for 30 min in the dark to reach an adsorption-desorption equilibrium between the photocatalyst and MB dye. Subsequently, the above mixture solution was irradiated in a photochemical chamber under continuously stirring with reflux water to keep its temperature constant. At certain time intervals, 3 mL solution was drawn out each time and centrifuged to get clear liquid. The quantitative determination of MB was performed by measuring its intensity of the absorption peak with a UV-vis spectrophotometer. Comparative experiments of degradation MB by using commercial ZnO and Ag_2O samples were also carried out.

Results and discussion

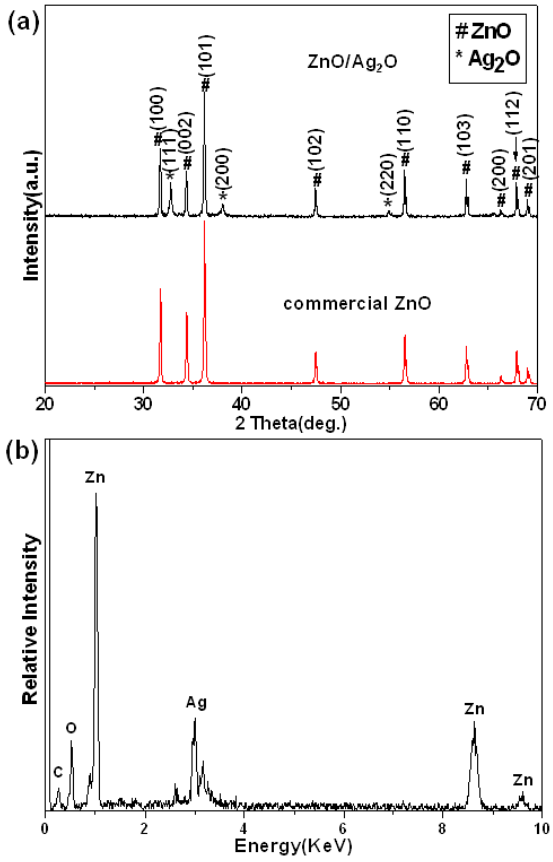

Fig. 1 XRD patterns of (a) commercial ZnO and the as-prepared ZnO/Ag_2O heterostructures, and EDS

spectrum of (b) the ZnO/Ag_2O.

Structure and Morphology

Fig. 1(a) shows the XRD patterns of commercial ZnO and the as-prepared ZnO/Ag_2O heterostructures. It can be found that all the diffraction peaks in the pattern of commercial ZnO can be indexed a hexagonal phase of wurtzite-type ZnO with lattice constants a = 3.249 Å and c = 5.206 Å, in accordance with the standard date (JCPDS Card No. 65-3411). In contrast, the nanocomposites exhibit three additional peaks at 32.8, 38.1, and 54.9, which can be indexed to the (111), (200), and (220) planes of Ag_2O, respectively (JCPDS Card No. 41-1104). No characteristic peaks for other impurities were observed, which indicated that the product had high purity. And the EDS analysis (Fig. 1(b)) further confirms that the product was only composed of O, Zn and Ag, except C which came from carbon conductive tap.

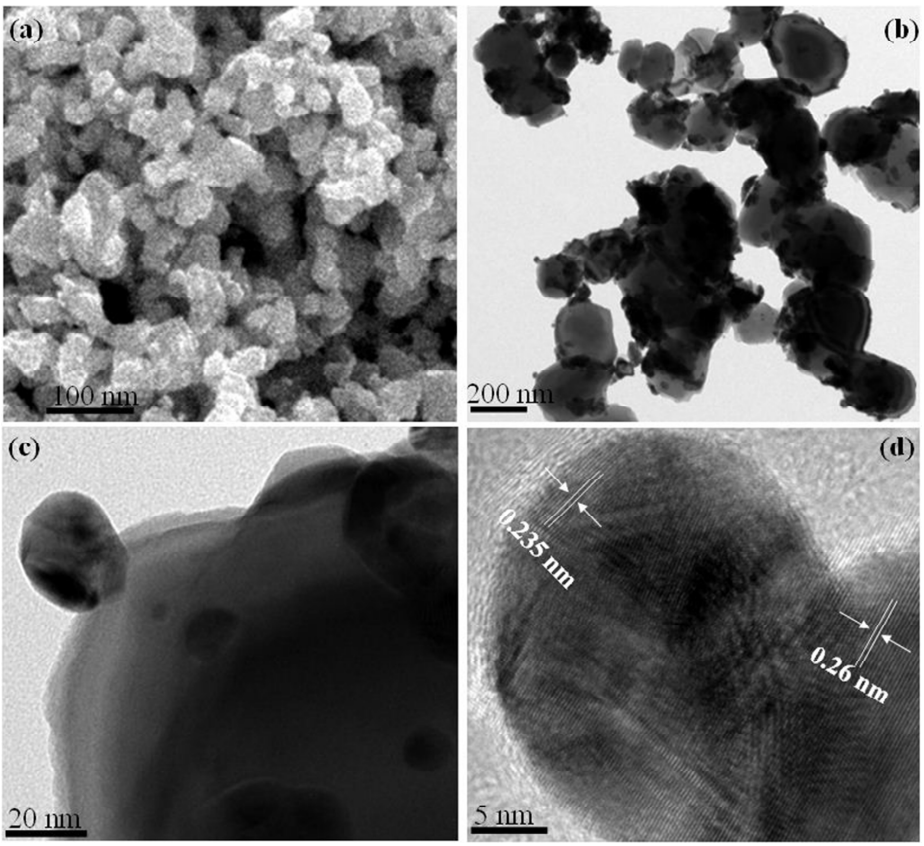

Fig. 2 (a) SEM image of the ZnO/Ag_2O heterostructures, and (b, c, and d) TEM and HRTEM images of the ZnO/Ag_2O heterostructures.

The morphologies of the as-prepared ZnO/Ag_2O heterostructures are shown in Fig. 2. Fig. 2(a , b) show the typical SEM images of the as-prepared ZnO/Ag_2O heterostructures, it can be found that the microstructure of the sample was composed of irregular nanoparticles with diameter of about 50-300 nm. Fig. 2(b) is a low-magnification TEM image of the ZnO/Ag_2O heterostructures. As can be seen, Ag_2O nanoparticles with a diameter range of 10-30 nm were coated on the surface of the ZnO nanoparticles. It is worth noting that the Ag_2O nanoparticles on ZnO nanoparticles are very stable and do not break off even when subjected to an ultrasonic treatment. From the HRTEM image of Fig. 2(c, d), the Ag_2O nanoparticles are tightly coupled on the surface of ZnO nanoparticles to form ZnO/Ag_2O

heterostructures, which is propitious to electron transmission between two phases. By measuring the lattice fringes in Fig. 2(d), the resolved interplanar distance of 0.26 nm agreed well with the lattice spacing of the (002) planes of the hexagonal wurtzite ZnO, and the interplanar distances of 0.235 nm, corresponding to the (200) plane of Ag_2O. These results also suggest that the as-prepared sample behaved as a well-crystallized heterostructure with ZnO nanoparticles and Ag_2O nanoparticles on nanoscale. In addition, the corresponding nitrogen adsorption-desorption isotherm of ZnO/Ag_2O heterostructures is shown in Fig. 3. The shape of the nitrogen isotherms exhibit type IV isotherm shape according to the IUPAC classification.[32] From the isotherm, the calculated BET surface area was 4.16 m^2/g, a total pore volume was 0.0207 cm^3/g, and an average pore diameter was 27.37 nm.

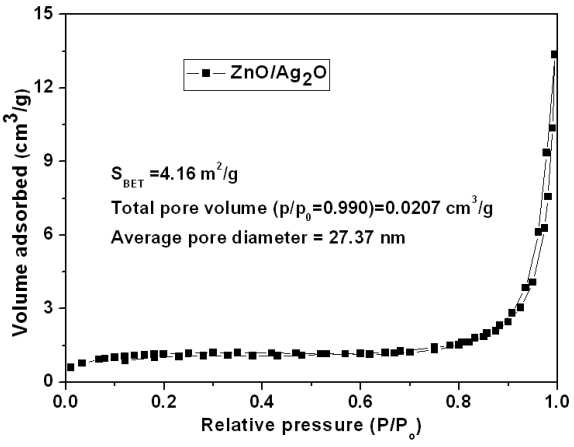

Fig. 3 N_2 adsorption-desorption isotherm of ZnO/Ag_2O heterostructures.

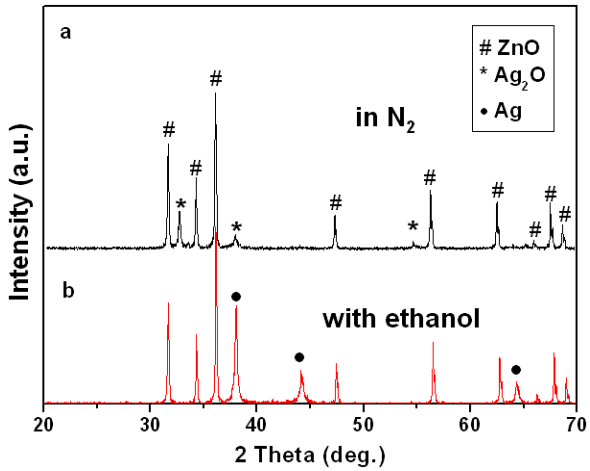

Fig. 4 XRD patterns of the samples synthesized under different experiment conditions: (a) with deionized water as the solvent under nitrogen atmosphere, (b) with ethanol as the solvent under air atmosphere.

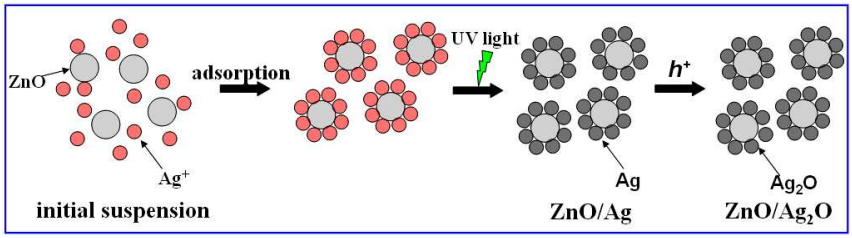

Scheme 1 Schematic illustration of the fabrication route of ZnO/Ag_2O heterostructures.

Formation mechanism of ZnO/Ag_2O heterostructures

In order to investigate the formation mechanism of the ZnO/Ag_2O heterostructures, different samples were synthesized under different experiment conditions and the XRD patterns are shown in Fig. 4 and Fig. S1. Fig. 4(a) shows the XRD pattern of the sample which was prepared with deionized water as the solvent in N_2 protection. It can be found that the phase of the sample was also ZnO/Ag_2O compared with the XRD pattern in Fig. 1(a). This result indicates that the Ag nanoparticles were not oxidized by O_2 in the reaction system. Furthermore, the ethanol was chosen as the solvent and synthesized another sample in air condition and the XRD pattern is shown in Fig. 4(b). As can be seen, the diffraction peaks of Ag_2O was disappeared and the peaks marked with "•" can be indexed to

face-centered-cubic metallic Ag (JCPDS Card No. 04-0783). This change may be attributed the ethanol solvent can acts as a hole scavenger to capture holes in the valence band and prevent recombination of the electron-hole pairs.[33] In addition, Fig. S1 show the XRD patterns of the samples synthesized in dark under different experiment conditions. As can be seen, no matter the products were synthesized with deionized water or ethanol in N_2 or air atmosphere, there are no obvious diffraction peaks of Ag or Ag_2O exist in the patterns while all the diffraction peaks only can be index of wurtzite-type ZnO. It indicates that the light is a necessary condition for the synthesis of ZnO/Ag_2O heterostructures. Therefore, On the basis of the above observations, a possible fabrication mechanism of the ZnO/Ag_2O heterostructures is proposed in Scheme 1. The ZnO surface is covered with a large number of hydroxyl groups and Ag^+ ions can adsorb onto the surface of the ZnO nanoparticles through electrostatic interaction that is sufficiently strong to prevent the silver nanoparticles aggregating. Under UV-light irradiation, the ZnO becomes excited and the photogenerated electrons (e^-) from the conduction band can reduce the Ag^+ ions to generate Ag atoms. Meanwhile, the photogenerated holes (h^+) are left in the valence band of ZnO. Subsequently, the Ag atoms can be oxidized to Ag_2O and the ZnO/Ag_2O heterostructures are formed.

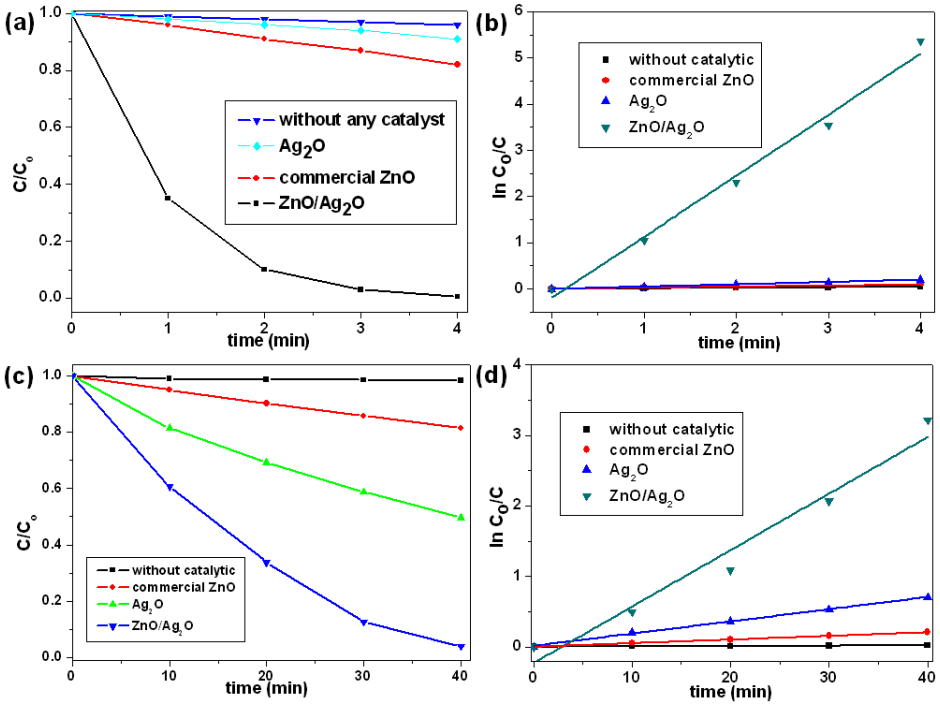

Fig. 5 Photocatalytic activity and kinetics of the as-prepared ZnO/Ag_2O heterostructures, commercial ZnO, and Ag_2O nanoparticles for degradation of MB: (a and b) under UV irradiation; (c and d) under visible light irradiation.

Photocatalytic Activity

The photcatalytic performances in UV and visible light regions were investigated via the degradation of MB, which is a typical cationic organic pollutant usually discharged by the textile industry after used. The photocatalytic activity and kinetics of the as-prepared ZnO/Ag_2O heterostructures, commercial ZnO, and Ag_2O nanoparticles for degradation of MB under UV and visible light irradiation are presented in Fig. 5. Fig. 5(a) shows the degradation rate of MB under UV irradiation without photocatalyst and using the as-prepared ZnO/Ag_2O heterostructures, commercial ZnO and Ag_2O nanoparticles, where C is the concentration of MB remaining in the solution after irradiation time t, and C_o is the initial concentration of MB. As can be seen, the self-degradation of MB (when there is no

sample added) does not change under high pressure mercury lamp irradiation for 4 min. The MB degradation rate for ZnO/Ag_2O heterostructures can reach 99.5% in 4 min under UV light irradiation, while the commercial ZnO and Ag_2O nanoparticles can only approach 18 % and 9 % for the same irradiation time, respectively. The photocatalysts degradation kinetic reaction can be described by pseudo-first-order kinetics, $\ln(C_o/C) = kt$, where k is a pseudo-first-rate kinetic constant and t is irradiation time. The variations in $\ln(C_o/C)$ as a function of irradiation time are given in Fig. 5(b). The calculate k value for the commercial ZnO and Ag_2O nanoparticles are 0.049 min^{-1} and 0.024 min^{-1}, respectively. And for as-prepared ZnO/Ag_2O heterostructures, the calculate k value is 1.34 min^{-1}, which is 27.4 times than bare commercial ZnO. It reveals that the photocatalysis activity of the composite is improved greatly because of the heterostructures between Ag_2O and ZnO.

Fig. 5(c, d) show the photocatalytic activity and kinetics of the as-prepared ZnO/Ag_2O heterostructures, commercial ZnO and Ag_2O nanoparticles for degradation of MB under visible light irradiation. Because of the large band gap energy (3.37 eV), ZnO photocatalysis proceed only at wavelengths shorter than approximately 400 nm. So, commercial ZnO has a low photocatalytic activity under visible light, and the degradation rate of MB is only 18.6 % in 40 min. The pure Ag_2O nanoparticles have a good visible-light photocatalytic activity and the degradation rate of MB reaches 51.4 % in 40 min. However, the as-prepared ZnO/Ag_2O heterostructures show a much better photocatalytic activity than that of the commercial ZnO and pure Ag_2O nanoparticles and the corresponding degradation rate can reach 96% in the same irradiation time. From Fig. 5(d), the calculate k value for as-prepared ZnO/Ag_2O heterostructures is 0.0847 min^{-1},

which is 15.6 times and 4.6 times than commercial ZnO (0.00514 min^{-1}) and pure Ag_2O nanoparticles (0.0175 min^{-1}), respectively. It demonstrates that Ag_2O nanoparticles also enhance the visible-light photocatalytic activity of the commercial ZnO. This result can be supported by the UV-vis diffuse reflectance spectra (DRS) of the commercial ZnO, pure Ag_2O nanoparticles and ZnO/Ag_2O heterostructures which are shown in Fig. S2. From Fig. S2, commercial ZnO exhibit a steep adsorption edge located at 380 nm. Ag_2O nanoparticles display strong capability of light absorption in both UV and visible light range of 200-650 nm in addition to the intrinsic absorption band derived from the band gap transition, which leads to good visible light photocatalytic activity. The UV-vis spectra of ZnO/Ag_2O heterostructures both exhibit a wide visible light absorption band around 400-650 nm and an absorption band in the UV region which assignable to the Zn-O bond. The absorption above 400 nm in ZnO/Ag_2O heterostructures in attributed to the presence of Ag_2O nanoparticles as visible-light sensitization, which has a strong and wide absorption band in the visible-light region.

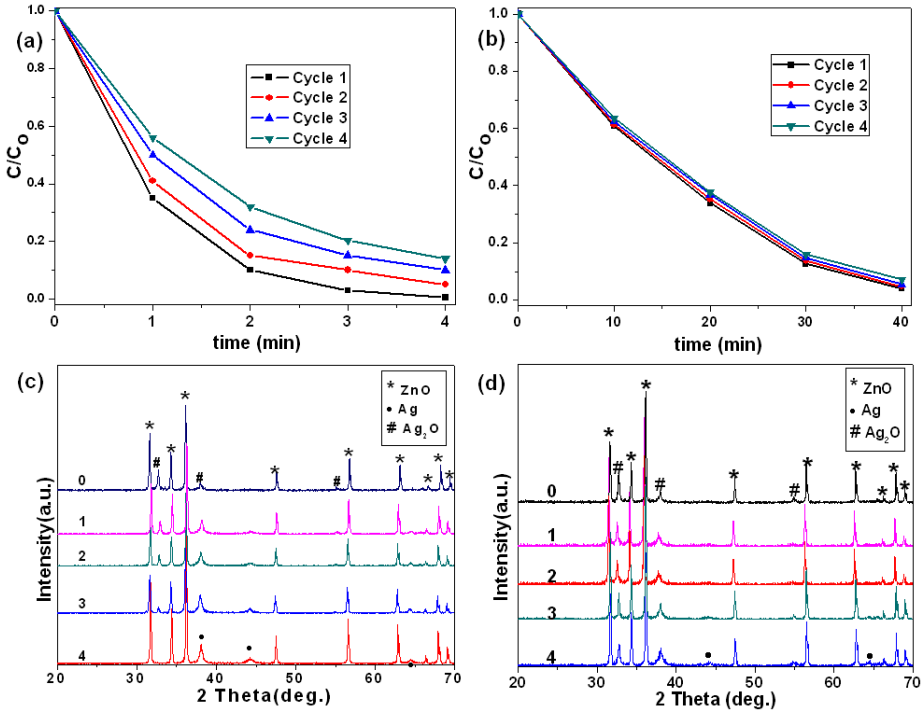

Fig. 6 Four photocatalytic degradation cycles of MB using ZnO/Ag_2O heterostructures under (a) UV, and (b) visible light irradiation, and the XRD patterns of the as-prepared ZnO/Ag_2O heterostructures after the repeated photocatalytic degradation experiments for four times under (c) UV, and (d) visible light irradiation.

To investigate the stability of photocatalytic performance in UV and visible light region, the as-prepared ZnO/Ag_2O heterostructures were used to degrade MB dye in four repeated cycles, and the results are shown in Fig. 6(a, b). It is noteworthy that the photocatalytic performance of the as-prepared ZnO/Ag_2O heterostructures exhibit effective photostability under visible light irradiation (Fig. 5(b)), where the photocatalytic efficiency reduces only by 3.2% after four cycles. However, as can be seen in Fig. 6(a), the ZnO/Ag_2O heterostructures is unstable for repeated use under UV irradiation. The photocatalytic activity of ZnO/Ag_2O heterostructures continuously decreased, and the photocatalytic degradation efficiency of MB is only 85.9% after repeatedly four times. To find the above reasons, we examined the XRD patterns of the ZnO/Ag_2O heterostructures at

the end of the repeated bleaching experiment under UV and visible light irradiation and the results are shown in Fig. 6(c, d). As seen from Fig. 6(c0), the ZnO/Ag_2O sample before UV irradiation is composed of ZnO and Ag_2O with high crystallinity. After repeated the first photocatalytic degradation of MB cycle under UV irradiation, the peaks corresponding to Ag are detected in the XRD pattern, which is shown in Fig. 6(c1). Significantly, the amount of Ag is continually increased with repeated times while the Ag_2O peaks are continually weakened. After cycle for four times, the Ag_2O peaks disappeared (Fig. 6(c4)), indicating structural transformation of Ag from Ag_2O phase during UV photocatalytic degradation experiments. Meanwhile, we also found the pure Ag_2O nanoparticles are almost stable under UV irradiation. The results suggest that Ag_2O can be destroyed by exposure to UV with the presence of ZnO. This is possible attributed to the Ag species are obtained from Ag_2O phase by electron reducing action of conduction band of ZnO under UV irradiation. In comparison with the XRD results under UV-light irradiation, the peak intensity and position of Ag_2O and ZnO of the as-prepared ZnO/Ag_2O heterostructures under visible-light irradiation shown in Fig. 6(d) maintain basically unchanged with increasing photocatalytic degradation time. However, from Fig. 6(d2-4), it is found that some very weak peaks corresponding to Ag are also detected. Under irradiation with visible light, only Ag_2O can be excited, and the photogenerated electrons on Ag_2O can partially reduce it to form Ag nanoparticles in situ. The results above imply that the reaction mechanism under visible-light irradiation is different from that under UV-light irradiation.

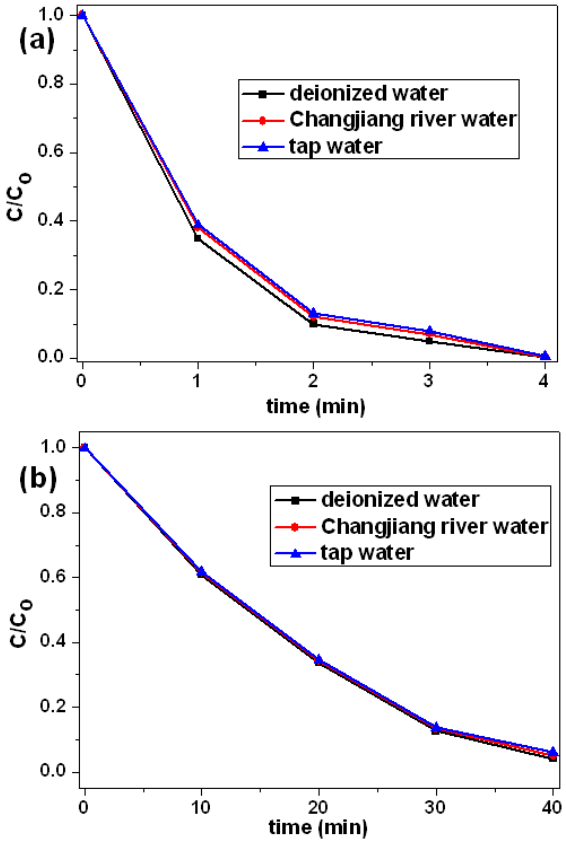

Fig. 7 Photocatalytic activity of the as-prepared ZnO/Ag_2O heterostructures for degradation of MB in different water sources under (a) UV irradiation; (b) visible light irradiation.

Fig. 7(a, b) show the photocatalytic activity of the as-prepared ZnO/Ag_2O heterostructures for degradation of MB in different water sources under UV and visible light irradiation, respectively. Firstly, MB was added into different water sources such as tap water and river water collected from Changjiang River in China to form several different MB solutions with the same concentration in deionized water. Then, the as-prepared ZnO/Ag_2O heterostructures were added into different MB solutions, followed by the same photocatalytic experiment steps above mentioned. As can be seen in Fig 7(a, b), the as-prepared ZnO/Ag_2O heterostructures almost exhibit the same photocatalytic activity in different water sources both under UV and visible light irradiation, suggesting that this

sample was suitable for removal of dyes from different water sources. It is also indicated that the as-prepared ZnO/Ag_2O heterostructures have great potential applications for pollution control in our environment.

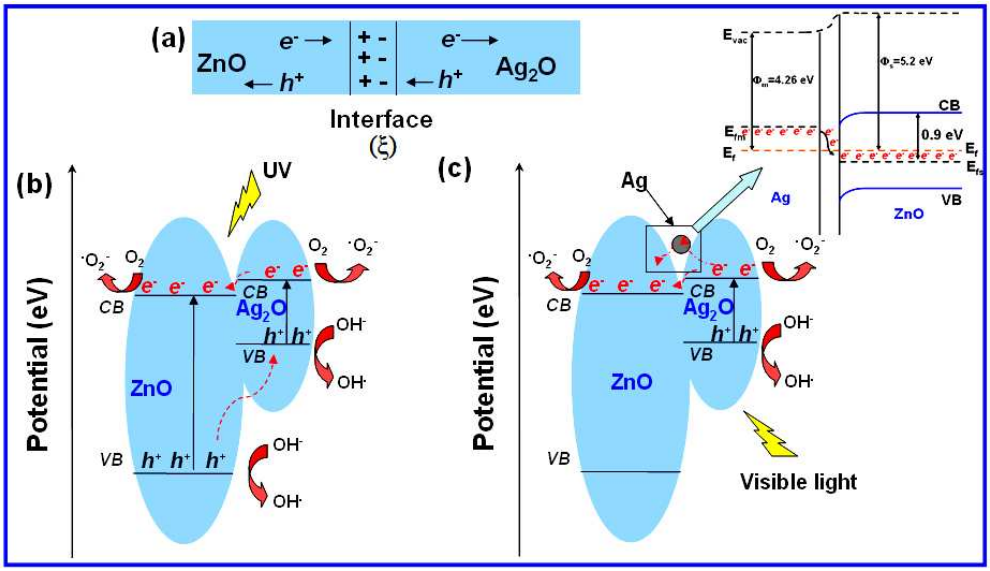

Fig. 8 (a) Schematic view for p-Ag_2O/n-ZnO heterojunction at equilibrium, and proposed photocatalytic mechanism of the as-prepared ZnO/Ag_2O heterostructures under (b) UV irradiation; (c) visible light irradiation. Inset of (c) is the corresponding band structures of Ag and ZnO junction and the Fermi energy level equilibrium with visible-light irradiation.

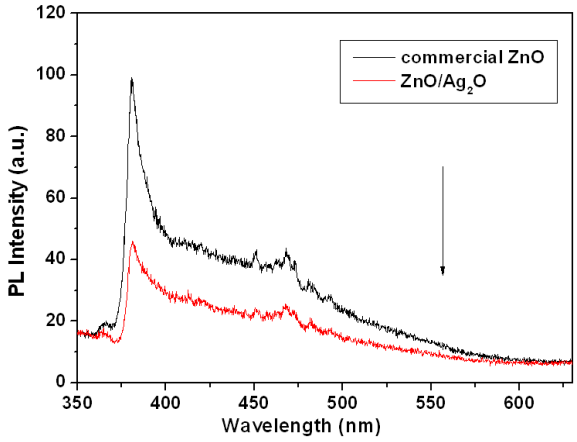

Fig. 9 PL emission spectra of commercial ZnO and ZnO/Ag_2O heterostructures.

Mechanisms in Enhancing Photocatalytic Activity

In order to fully understand the loading effects of Ag_2O nanoparticles on ZnO nanoparticles, it is necessary to obtain further information about the energy band of Ag_2O and ZnO. Ag_2O is a p-type narrow band gap semiconductor with ionization potential of 5.3 eV[34] and work function of 5.0 eV,[35] while wurtzite ZnO is a n-type wide band gap semiconductor with electron affinity of 4.3 eV and work function of 5.2 eV.[36] The Fermi level is the chemical potential of thermodynamic equilibrium, and ZnO and Ag_2O semiconductors have generally different positions of Fermi levels when they are separated or pre-equilibrium.[37] When Ag_2O nanoparticles are attached onto the ZnO nanoparticles surface, the p-n nanoheterojunctions are formed at the interface and electron transfer occurred from ZnO to Ag_2O until their Fermi levels align; i. e., the semiconductor system reaches the thermal equilibrium state.[38,39] Because of carrier concentration gradients, electrons diffuse from n-type to p-type region and holes diffuse from the p-type to n-type region which is shown in Fig. 8(a). At the junction in equilibrium, the n-type ZnO regions have a positive charge, while p-type Ag_2O has a negative charge, so that an opposing electric field (ξ) is created at the junction and there is an equilibrium potential difference across the transition region, called contact potential. During the photocatalysis process, the photogenerated electrons can move to the conduction band of the n-type ZnO and holes can move to the valence band of the p-type Ag_2O due to the built in electric field at the p-Ag_2O/n-ZnO nanojunction and retard the recombination. On the basis of above values, a possible mechanism of high photocatalytic activities of ZnO/Ag_2O heterostructures under UV and visible-light irradiation is shown in Fig. 8(b and c). Meanwhile, the relevant formula reactions are shown as following:

$$ZnO(s) + h\nu \rightarrow ZnO(s) + e^- + h^+$$

$$Ag_2O(s) + h\nu \rightarrow Ag_2O(s) + e^- + h^+$$

$$Ag_2O(s) + e^- \rightarrow Ag\ (s) + O_2$$

$$e^- + O_2 \rightarrow O_2\cdot^-$$

$$O_2\cdot^- + H_2O \rightarrow HO_2\cdot + OH\cdot$$

$$HO_2\cdot + H_2O \rightarrow H_2O_2 + OH\cdot$$

$$H_2O_2 \rightarrow 2OH\cdot$$

$$h^+ + OH^- \rightarrow OH\cdot$$

$$OH\cdot + MB\ (dye) \rightarrow CO_2 + H_2O$$

$$h^+ + MB\ (dye) \rightarrow CO_2 + H_2O$$

Under UV-light irradiation, both ZnO (3.37 eV) nanoparticles and Ag_2O (1.2 eV) nanoparticles are simultaneously excited to produced h^+ and e^-.[40,41] Under normal case, most of electrons-holes pairs recombine rapidly and thus the commercial ZnO nanoparticles have a low photocatalytic activity. Herein, as shown in Fig. 8(b), due to band banding and under the influence of the electrostatic field ξ in the junction, the photogenerated electrons easily transfer from the CB of Ag_2O to that of ZnO and holes transfer from the VB of ZnO to that of Ag_2O, suggesting that the photogenerated electrons and holes were efficiently separated. Furthermore, the better separation of photogenerated electrons and holes in the p-type Ag_2O and n-type ZnO heterojunction was confirmed by comparing the PL spectra of the commercial ZnO and ZnO/Ag_2O heterostructures. The PL spectrum is related to the transfer behavior of the photogenerated electrons and holes, so that it can reflect the separation and recombination of photogenerated charge carriers.[42] The PL spectra of

commercial and ZnO are shown in Fig. 9. As can be seen, the ZnO/Ag_2O heterostructures exhibit much lower emission intensity than commercial ZnO, indicating that the recombination of the photogenerated charge carrier was inhibited greatly in the p-type Ag_2O and n-type ZnO heterojunction. Thus, the lifetime of the excited electrons and holes can be prolonged in the transfer process, inducing higher quantum efficiency, and thus the photocatalytic activity of the as-prepared ZnO/Ag_2O heterostructures is enhanced greatly. Subsequently, the photogenerated electrons react with adsorbed O_2 and H_2O on the surface of the heterostructures and produce superoxide radical anions such as $O_2^{-}\bullet$. The photogenerated holes can be trapped by H_2O and OH^- to further produce •OH species, which is a strong oxidizing agent.[21] Meanwhile, the generated O_2 from Ag_2O-loaded photocatalysts promote to produce more reactive oxygen species ·OH, which also improve the photocatalytic activity under UV-light irradiation.

When the as-prepared ZnO/Ag_2O heterostructures are irradiated with visible light, only Ag_2O can be excited due to its narrow band gap (1.2 eV). And the photogenerated electrons are produced in the CB while the photogenerated holes (h^+) remain in the VB. The photogenerated electrons easily transfer from the CB of Ag_2O to that of ZnO due to the band banding and the influence of the electrostatic field ξ in the junction, suggesting that the photogenerated electrons and holes could be separated efficiently. Moreover, in view of the more positive potential of Ag^+/Ag (0.7991 V, vs. SHE) compared with O_2/HO_2 (-0.046 V, vs. SHE), the photogenerated electrons are preferably transferred to the lattice Ag^+.[34] Actually, the Ag^+ ion has been demonstrated to be an effective sacrificial reagent to capture photogenerated electrons for the evolution of oxygen during the splitting of water.[43] In this

study, the partial content of Ag^+ in Ag_2O was reduced in situ by photogenerated electrons and formed metallic Ag during the photocatalytic cycle experiments as suggested by the detectable diffraction peak of Ag in Fig. 6(d). Once a certain amount of metallic Ag is formed on the surface of Ag_2O, the following photogenerated electrons tend to transfer to the metallic-Ag sites.[44] Where after, as shown inset of Fig. 8(c), the work function of Ag is about 4.26 eV, thus, the Fermi energy level of ZnO (E_{fs}) is lower than that of Ag (E_{fm}) because of the larger work function of ZnO, resulting in the transfer of electrons from Ag to ZnO until the two systems attain equilibrium and form the new Fermi energy (E_f)[36, 45] and the recombination of electron-hole pairs are then reduced. Meanwhile, metal (Ag) and semiconductor (ZnO and Ag_2O) would form Schottky barriers at their interfaces because of their difference in work function and band alignment, leading to the obvious separation and transfer of photoexcited charges.[46] Thus, the photocatalytic activity of the as-prepared ZnO/Ag_2O heterostructures under visible-light is enhanced.

Conclusions

In summary, the ZnO/Ag_2O heterostructures had been successfully fabricated via the photochemical technique rout. The as-prepared ZnO/Ag_2O heterostructures had shown significant enhanced photocatalytic activity toward MB degradation under UV and visible light irradiation than that of pure ZnO and Ag_2O nanoparticles. Under UV-light irradiation, Ag_2O nanoparticles act as an electron absorbing agent scavenged the valence electrons of ZnO nanoparticles to enhance electron-hole separation. Under visible-light irradiation, the enhanced photocatalytic activity could be attributed to the partial formation of metallic Ag

on the surface of Ag_2O nanoparticles during the photodecomposition of organic substances. The metallic Ag nanoparticles act as an electron absorbing agent scavenged the valence electrons of Ag_2O nanoparticles. Then the electrons on Ag nanoparticles migrate to the CB of ZnO according to the larger work function of ZnO, resulting in the reduction of the recombination of electron-hole pairs. Furthermore, the as-prepared ZnO/Ag_2O heterostructures could also degrade MB dye in different water sources like Changjiang river water and tap water with high efficiency as well as in deionized water both under UV and visible-light irradiation. Thus, the ZnO/Ag_2O heterostructures is a promising candidate for the removal of hazardous organic materials from wastewater.

Acknowledgements

The authors are grateful to National Natural Science Foundation of China (Grant No.21106017 and 51077013), Fund Project for Transformation of Scientific and Technological Achievements of Jiangsu Province of China (Grant No. BA2011086), Specialized Research Fund for the Doctoral Program of Higher Education of China (Grant No.20100092120047) and Key Program for the Scientific Research Guiding Found of Basic Scientific Research Operation Expenditure of Southeast University(Grant No.3207042102)

Reference

1. J. M. Hall-Spencer, R. Rodolfo-Metalpa, S. Martin, E. Ransome, M. Fine, S. M. Turner, S. J. Rowley, D. Tedesco and M. C. Buia, *Nature*, 2008, **454**, 96-99.

2. M. A. Shannon, P. W. Bohn, M. Elimelech, J. G. Georgiadis, B. J. Marinas and A. M. Mayes, *Nature*, 2008, **452**, 301-310.

3. C. J. Vorosmarty, P. B. McIntyre, M. O. Gessner, D. Dudgeon, A. Prusevich, P. Green, S. Glidden, S. E. Bunn, C. A. Sullivan, C. R. Liermann and P. M. Davies, *Nature*, 2010, **468**, 334-334.

4. M. R. Hoffmann, S. T. Martin, W. Y. Choi and D. W. Bahnemann, *Chem. Rev.*, 1995, **95**, 69-96.

5. L. L. Li, Y. Chu, Y. Liu and L. H. Dong, *J. Phys. Chem. C*, 2007, **111**, 2123-2127.

6. Y. R. Smith, A. Kar and V. Subramanian, *Ind. Eng. Chem. Res.*, 2009, **48**, 10268-10276.

7. C. H. Wang, C. L. Shao, Y. C. Liu and X. H. Li, *Inorg. Chem.*, 2009, **48**, 1105-1113.

8. L. S. Zhang, W. Z. Wang, J. O. Yang, Z. G. Chen, W. Q. Zhang, L. Zhou and S. W. Liu, *Appl. Catal. a-Gen*, 2006, **308**, 105-110.

9. A. B. Djurisic, X. Y. Chen, Y. H. Leung and A. M. C. Ng, *J. Mater. Chem.*, 2012, **22**, 6526-6535.

10. L. Q. Jing, D. J. Wang, B. Q. Wang, S. D. Li, B. F. Xin, H. G. Fu and J. Z. Sun, *J. Mol. Catal. a-Chem.*, 2006, **244**, 193-200.

11. F. Xu, Y. T. Shen, L. T. Sun, H. B. Zeng and Y. N. Lu, *Nanoscale*, 2011, **3**, 5020-5025.

12. C. Q. Zhu, B. A. Lu, Q. Su, E. Q. Xie and W. Lan, *Nanoscale*, 2012, **4**, 3060-3064.

13. Q. Deng, X. W. Duan, D. H. L. Ng, H. B. Tang, Y. Yang, M. G. Kong, Z. K. Wu, W. P. Cai and G. Z. Wang, *Acs Appl. Mater. Inter.*, 2012, **4**, 6030-6037.

14. X. B. Cao, X. M. Lan, Y. Guo, C. Zhao, S. M. Han, J. Wang and Q. R. Zhao, *J. Phys. Chem. C*, 2007, **111**, 18958-18964.

15. H. B. Fu, T. G. Xu, S. B. Zhu and Y. F. Zhu, *Environ. Sci. Technol.*, 2008, **42**, 8064-8069.

16. R. Ostermann, D. Li, Y. D. Yin, J. T. McCann and Y. N. Xia, *Nano Lett.*, 2006, **6**, 1297-1302.

17. Q. Wang, B. Y. Geng and S. Z. Wang, *Environ. Sci. Technol.*, 2009, **43**, 8968-8973.

18. H. B. Zeng, P. S. Liu, W. P. Cai, S. K. Yang and X. X. Xu, *J. Phys. Chem. C*, 2008, **112**, 19620-19624.

19. A. L. Linsebigler, G. Q. Lu and J. T. Yates, *Chem. Rev.*, 1995, **95**, 735-758.

20. H. Gu, Y. Yang, J. X. Tian and G. Y. Shi, *Acs Appl. Mater. Inter.*, 2013, **5**, 6762-6768.

21. C. L. Yu, K. Yang, Y. Xie, Q. Z. Fan, J. C. Yu, Q. Shu and C. Y. Wang, *Nanoscale*, 2013, **5**, 2142-2151.

22. Y. J. Wang, Q. S. Wang, X. Y. Zhan, F. M. Wang, M. Safdar and J. He, *Nanoscale*, 2013, **5**, 8326-8339.

23. Z. B. Yu, Y. P. Xie, G. Liu, G. Q. Lu, X. L. Ma and H. M. Cheng, *J. Mater. Chem. A*, 2013, **1**, 2773-2776.

24. Z. Wang, S. W. Cao, S. C. J. Loo and C. Xue, *Crystengcomm*, 2013, **15**, 5688-5693.

25. C. W. Zou, Y. F. Rao, A. Alyamani, W. Chu, M. J. Chen, D. A. Patterson, E. A. C. Emanuelsson and W. Gao, *Langmuir*, 2010, **26**, 11615-11620.

26. M. Wu, J. M. Yan, M. Zhao and Q. Jiang, *Chempluschem*, 2012, **77**, 931-935.

27. X. Wang, H. F. Wu, Q. Kuang, R. B. Huang, Z. X. Xie and L. S. Zheng, *Langmuir*, 2010, **26**, 2774-2778.

28. J. Roithova and D. Schroder, *J. Am. Chem. Soc.*, 2007, **129**, 15311-15318.

29. Y. Xu, M. Schoonen, *Mineral*, 2010, **85**, 543-556.

30. D. Sarkar, C. K. Ghosh, S. Mukherjee and K. K. Chattopadhyay, *Acs Appl. Mater. Inter.*, 2013, **5**, 331-337.

31. L. L. Xu, B. Wei, W. L. Liu, H. L. Zhang, C. Y. Su and J. X. Che, *Nanoscale Res. Lett.*, 2013, **8**, 536.

32. K. S. W. Sing, D. H. Everett, R. A. W. Haul, L. Moscou, R. A. Pierotti, J. Rouquerol and T. Siemieniewska, *Pure Appl. Chem.*, 1985, **57**, 603-619.

33. H. Y. Li, W. B. Lu, J. Q. Tian, Y. L. Luo, A. M. Asiri, A. O. Al-Youbi and X. P. Sun, *Chem. Eur. J.*, 2012, **18**, 8508-8514.

34. S. Y. Ryu, J. H. Noh, B. H. Hwang, C. S. Kim, S. J. Jo, J. T. Kim, H. S. Hwang, H. K. Baik, H. S. Jeong, C. H. Lee, S. Y. Song, S. H. Choi and S. Y. Park, *Appl. Phys. Lett.*, 2008, **92**, 023306-1-023306-3.

35. H. W. Choi, S. Y. Kim, K. B. Kim, Y. H. Tak and J. L. Lee, *Appl. Phys. Lett.*, 2005, **86**, 012104-012104-3.

36. W. W. Lu, S. Y. Gao and J. J. Wang, *J. Phys. Chem. C*, 2008, **112**, 16798-16800.

37. M. Grundmann, *The Physics of Semiconductors*, Springer-Verlag, Heidelberg, 2006.

38. M. T. Mayer, C. Du and D. W. Wang, *J. Am. Chem. Soc.*, 2012, **134**, 12406-12409.

39. N. Liang, J. T. Zai, M. Xu, Q. Zhu, X. Wei and X. F. Qian, *J. Mater. Chem. A*, 2014, **2**, 4208-4216.

40. W. J. Zhou, H. Liu, J. Y. Wang, D. Liu, G. J. Du and J. J. Cui, *Acs Appl. Mater. Inter.*, 2010, **2**, 2385-2392.

41. A. J. Bard, R. Parsons, J. Jordan, *Standard Potentials in Aqueous Solution*, Marcel Dekker, New York, 1985.

42. H. B. Zeng, G. T. Duan, Y. Li, S. K. Yang, X. X. Xu and W. P. Cai, *Adv. Funct. Mater.*, 2010, **20**, 561-572.

43. A. Kudo, H. Kato and I. Tsuji, *Chem. Lett.*, 2004, **33**, 1534-1539.

44. X. F. Wang, S. F. Li, H. G. Yu, J. G. Yu and S. W. Liu, *Chem. Eur. J.*, 2011, **17**, 7777-7780.

45. D. D. Lin, H. Wu, R. Zhang and W. Pan, *Chem. Mater.*, 2009, **21**, 3479-3484.

46. H. B. Zeng, W. P. Cai, P. S. Liu, X. X. Xu, H. J. Zhou, C. Klingshirn and H. Kalt, *ACS Nano*, 2008, **2**, 1661-1670.